

# We are IntechOpen, the world's leading publisher of Open Access books Built by scientists, for scientists

6,900

Open access books available

185,000

International authors and editors

200M

Downloads

Our authors are among the

154

Countries delivered to

TOP 1%

most cited scientists

12.2%

Contributors from top 500 universities



WEB OF SCIENCE™

Selection of our books indexed in the Book Citation Index  
in Web of Science™ Core Collection (BKCI)

Interested in publishing with us?  
Contact [book.department@intechopen.com](mailto:book.department@intechopen.com)

Numbers displayed above are based on latest data collected.  
For more information visit [www.intechopen.com](http://www.intechopen.com)



# Synthesis, Structural and Thermal Properties of Nano-porous SiO<sub>2</sub>-based Aerogels

Hexin Zhang<sup>1</sup>, Changqing Hong<sup>2</sup> and Yingjie Qiao<sup>1</sup>

<sup>1</sup>*College of Materials Science and Chemical Engineering,  
Harbin Engineering University,*

<sup>2</sup>*Center for Composite Materials and Structure,  
Harbin Institute of Technology,  
PR China*

## 1. Introduction

Nano-porous silica aerogels are unique materials often having a high specific surface area, a high porosity (75-99%), a low thermal conductivity (0.01-0.03W/mK), and a low index of refraction. Because of their unique properties, aerogels have been extensively studied, not only for use as transparent thermal insulators but also as inter-metal dielectric materials, optical and acoustic applications, and the space industry (Muller et.al, 1999; Hrubesh et.al, 2001; Kim & Hyun, 2003; Lu et.al, 1991). NASA has applied aerogel on the Mars Pathfinder Sojourner rover and Mars Exploration rovers for insulation purposes. Additional applications of aerogels are found in battery electrodes, catalysts and electronic devices (Fricke et.al, 1992; Fricke & Tillotson, 1997; Kuhn et.al, 1995; Chadwick et.al, 2001).

Currently SiO<sub>2</sub>, Al<sub>2</sub>O<sub>3</sub> and C aerogels are reported and available elsewhere. During the production of aerogel a wet gel is formed which dried becomes filled with air. An aerogel is made up of microscopic beads or strand chains connected to form a continuous network, it is considered a solid. The fact that typical aerogels have more than 90% porosity gives them unusual characteristics (Yoda et.al, 1998; Klementiev, 2001). Their structure is composed of a 3-D connected network of channels made of thin ligaments. The thickness of ligaments determines the final density and porosity of the aerogel (Reim et al, 2004; Kwon & Choi, 2000).

As for thermal insulation application, generally monolithic SiO<sub>2</sub> aerogels provide a whole low thermal conductivity due to its extremely high porosity. The thermal conductivity of aerogels is about 100 times smaller than that of full density silica glass, although Kistler made initial thermal conductivity measurements, a detailed understanding of thermal transport in aerogel resulted from investigations carried out (Fricke & Tillotson, 1997). Thermal transport in aerogel occurs via gaseous conductivity, solid conductivity and infrared radiative transfer. Usually at room temperature, aerogels have a low thermal conductivity due to its special gas conduction and solid conduction. However, at higher temperatures, radiative absorption/emission becomes the dominant heat transfer mechanism.

Monolithic aerogel behaves poor thermal insulation because it is highly transparent in the 3-8 $\mu$ m wavelength region. To improve its thermal insulation capacity, approaches such as doping aerogel with carbon have been applied to minimize infrared radiation heat transfer. The specific extinction for C doped aerogels is drastically increased, especially in the 2 to

8 $\mu\text{m}$  range. Carbon black doped aerogel beads have total thermal conductivity of about 0.020  $\text{Wm}^{-1}\text{K}^{-1}$  in air, while for monoliths approximately 0.015  $\text{Wm}^{-1}\text{K}^{-1}$  holds (Zhang et.al, 2009). The opacified fibers also suppress radiation transport by eliminating the infrared transparent window of aerogel and strengthen the brittle monolithic aerogel when fibers are incorporated into the aerogel matrix. Therefore, an appropriate selection of fiber type and concentration is critical to optimizing the thermal insulation capacity of the material, especially at high temperatures.  $\text{K}_2\text{Ti}_6\text{O}_{13}$  whisker is an efficient opacifier due to its high-reflection index, thermal stability and negative temperature coefficient; therefore it drastically reduces the radiative heat transfer in the prepared  $\text{SiO}_2$  aerogels. Additionally  $\text{TiO}_2$  is also a good opacifier due to its high reflection index, thermal stability and strong broad band absorber. The specific extinction of the opacified aerogel is drastically increased, especially in the range from 2 to 8  $\mu\text{m}$  (Wang, et.al, 1995).

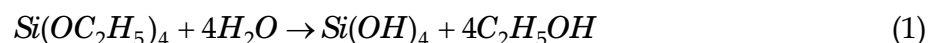
## 2. Production of aerogels

### 2.1 Silica aerogels

Since the actual applications for aerogels are virtually unlimited, they will have to be cheaply manufactured in order to have an impact in the commercial marketplace. As such, many researchers have now paid their attention to achieving these goals. Some research institutions have designed methods to eliminate the supercritical drying process and the high capital cost associated with it, while others have begun to make it more efficient. Practicing results have revealed that the high cost of the raw materials contributes significantly to the final cost of the aerogel.

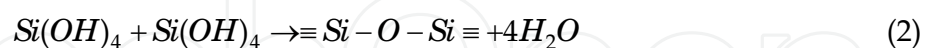
Usually Silica aerogels were prepared by hydrolysis and polycondensation of solvent (alcohol) diluted alkoxide in the presence of a catalyst. The hydrolysis and polycondensation reaction mechanism for tetraethoxysilane (TEOS) precursor is as given below:

Hydrolysis:



A catalyst (Critic acid) is used here.

Condensation:



Similarly, tetramethoxysilane (TMOS) and polyethoxydisiloxane (PEDS) precursors follow the same trend of chemical reactions. There are some structural differences among TEOS, TMOS and PEDS, although the reactive mechanism is similar during the process of hydrolysis and condensation. Figure.1 lists the pore size distribution using TEOS, TMOS and PEDS as precursors.

From the present studies, it has been found that the precursors: TEOS, TMOS and PEDS strongly affect the physical properties like bulk density, percentage of porosity, pore size distribution, optical transmission, surface area, thermal conductivity and microstructure of silica aerogels. Table.1 shows the effect of various precursors on some physical properties of silica aerogels.

Precursor	Optimized molar ratio: Solvent: water	Catalyst	Gelation time	Bulk density (Kg m <sup>-3</sup> )	Porosity (%)	Surface area (m <sup>2</sup> gm <sup>-1</sup> )	Thermal Conductivity (Wm <sup>-1</sup> K <sup>-1</sup> )
TEOS	TEOS:EtOH:H <sub>2</sub> O 1:5:7	Citric acid 0.001M	2.2days	230	87.89	800	0.060
TMOS	TMOS:MeOH:H <sub>2</sub> O 1:12:4	NH <sub>4</sub> OH 0.05M	30min	129	93.21	1000	0.020
PEDS	PEDS:EtOH:H <sub>2</sub> O 1:5:6	HF 0.01M	10min	98	96.84	1100	0.015

Table 1. Effect of various precursors on some physical properties of silica aerogels. Ref (Wagh,et al, 1999)

The experimental results showed that TMOS and PEDS aerogels has high surface areas of 1000 and 1100 m<sup>2</sup>gm<sup>-1</sup>, respectively. While, TEOS aerogel possesses low (800 m<sup>2</sup>gm<sup>-1</sup>) surface area compared to the TMOS and PEDS aerogels. This is due to the fact that both the TMOS and PEDS aerogels consist of smaller size SiO<sub>2</sub> particles of the network whereas TEOS aerogels consists of larger size SiO<sub>2</sub> particles of the network as explained earlier. The thermal conductivity of the TEOS aerogels measured at room temperature has been found to be 0.06 Wm<sup>-1</sup>K<sup>-1</sup> whereas the thermal conductivity values for TMOS and PEDS aerogels have been found to be 0.02 and 0.015 Wm<sup>-1</sup>K<sup>-1</sup>, respectively. This is due to the fact that the density of the TEOS aerogel is higher (230 Kg m<sup>-3</sup>) compared to the densities of TMOS (129 Kg m<sup>-3</sup>) and PEDS (98 Kg m<sup>-3</sup>) aerogels. The dependence of thermal conductivity as a function of density is explained in the results.

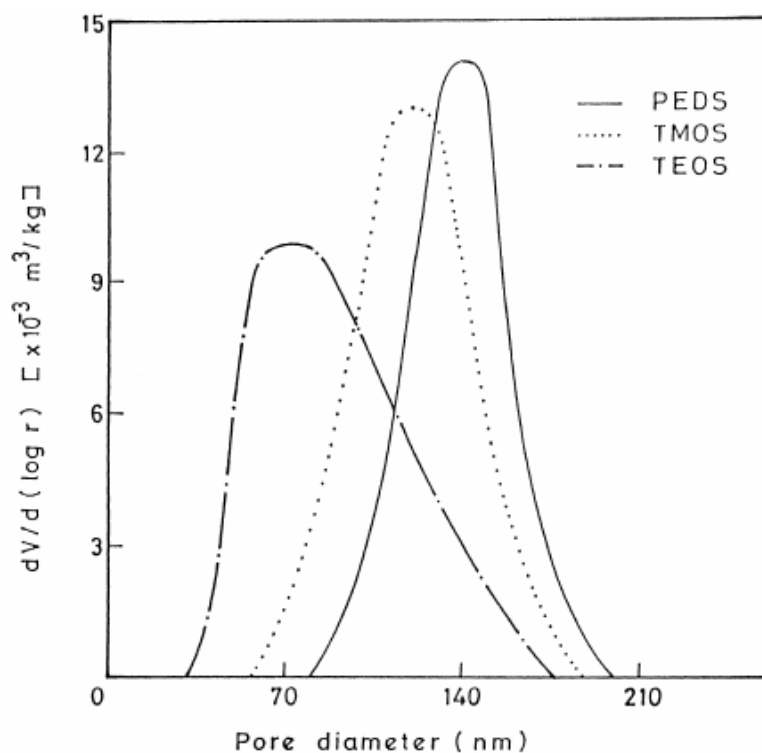


Fig. 1. Pore size distributions (PSDs) of silica aerogels for various precursors: TEOS, TMOS and PEDS. Ref.(Wagh,et al, 1999)

Aerogels are often produced by the supercritical extraction of pore liquid from wet gels, which limits industrial-scale production of aerogels. Silica aerogels were recently prepared at an ambient pressure through solvent exchange and surface modification of wet gels. Solvent exchange and surface modification are essential to preserve the porous network of the gel before ambient pressure drying. Usually, under the condition of an ambient pressure drying, surface-modified agent is required. To modify the surface of the gel, a simultaneous solvent exchange and surface modification process at ambient pressure is needed to reduce the time required for synthesis from several days and to reduce shrinkage during drying.

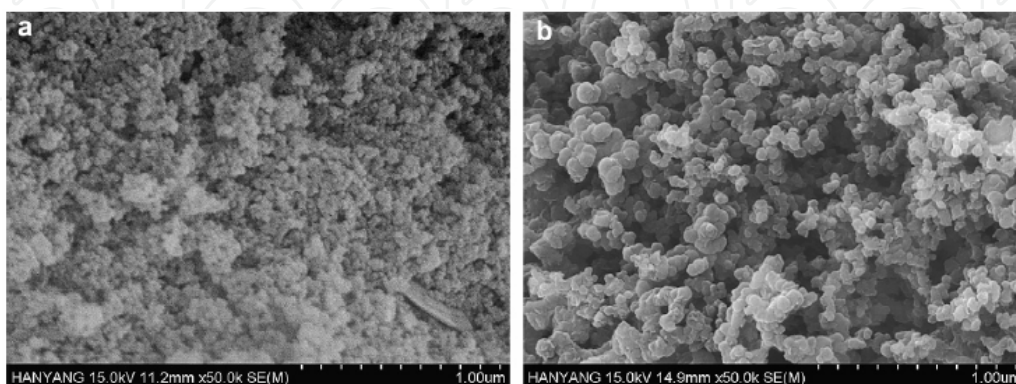


Fig. 2. FE-SEM micrograph of (a) unmodified and (b) TMCS modified (10%V of TMCS) mesoporous silica beads. Ref (Sarawade et al, 2010)

Figure.2 shows the pore characteristics and structure morphology of mesoporous silica beads based on SEM micrographs of unmodified and 10%V TMCS modified silica beads. In general, the unmodified silica beads formed dense aggregates of spheres while the modified silica beads had highly porous structure. This is because the unmodified wet gel silica beads shrank more during ambient pressure drying, resulting in dense aggregates of dried silica beads and the loss of mesopores. The samples modified with TMCS had mesopores with an average pore diameter in the range of 8-13 $\mu$ m. This is due to the fact that reversible shrinkage occurred in the wet gel silica during drying because of organic modification of the surface with trimethyl groups.

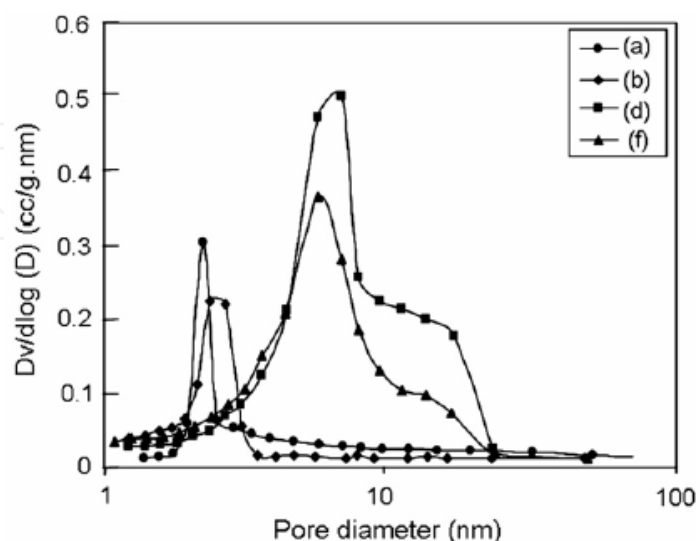


Fig. 3. Pore size distributions of (a) unmodified silica beads together with those modified with (b) 2 (d) 6 and (f) 10%V of TMCS. Ref (Sarawade et al, 2010)

Figure.3 shows the pore size distribution of unmodified and modified silica aerogels. Unmodified silica beads have a narrow pore size distribution with a peak pore diameter of 6.1 nm. Modified silica beads had a broad pore size distribution with the peak pore diameters ranging from 8 to 13 nm. The peak pore diameter increased as the volume of TMCS increased from 2 to 10%. This enlargement of pores is considered to be due to the increase in non-polar alkyl groups (-CH<sub>3</sub>) on the silica surface, which reduces shrinkage during drying and therefore increases pore size. As per the IUPAC classification of pores, all the silica beads showed a pronounced peak in the mesopore region (2-50 nm) indicating that the mesopores in the modified silica beads have remained intact, even after the drying process.

During synthesizing SiO<sub>2</sub> aerogels, modification solvent plays an important role in determining the final microstructure. In our previous studies, cyclohexane was selected for surface modification of SiO<sub>2</sub> aerogel using TEOS as precursor before ambient pressure drying. Figure.4 showed the unmodified and modified micro-morphology using cyclohexane as solvent exchange. The unmodified silica aerogel formed some aggregates of spheres while the modified silica aerogel had porous structure with high porosity. These results might be identical to that of Ref(Sarawade et al, 2010).

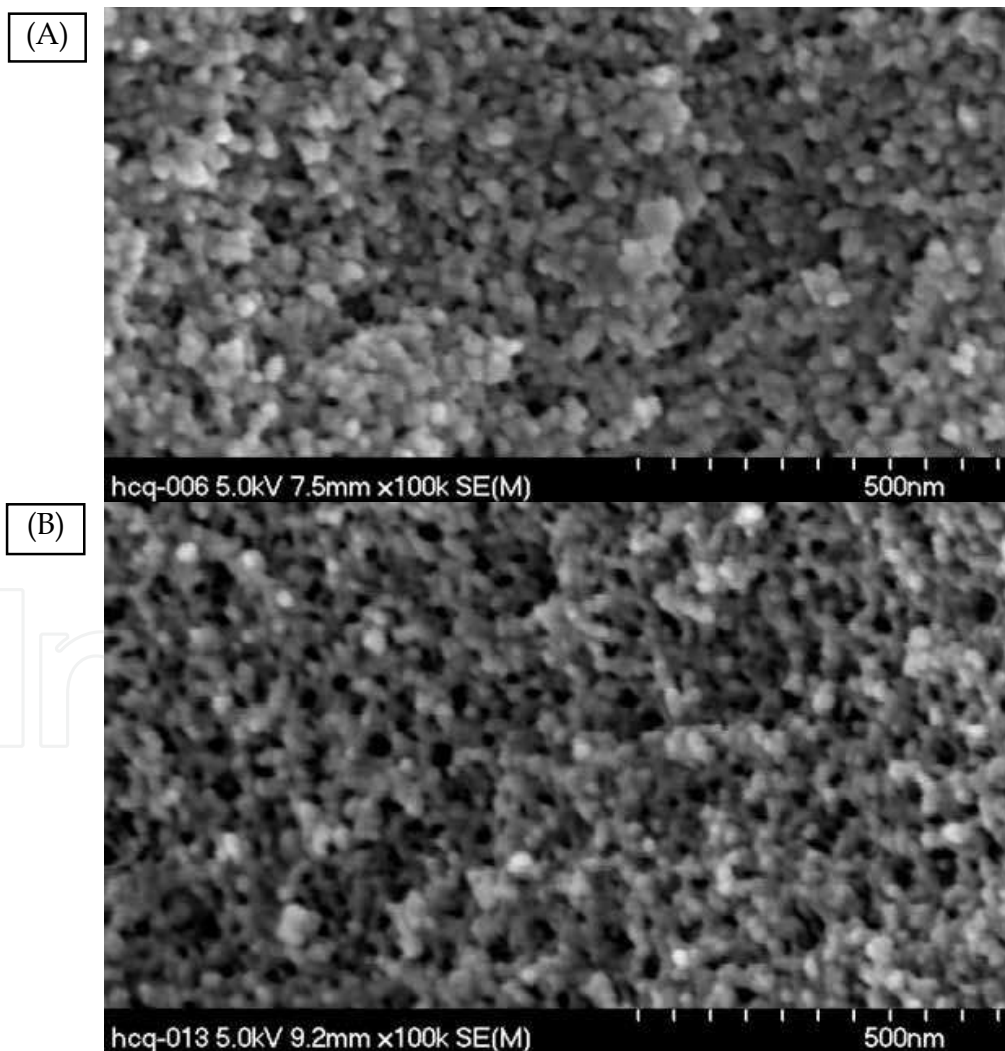


Fig. 4. SEM micrograph of (A) unmodified and (B) cyclohexane modified mesoporous silica aerogels

## 2.2 Carbon aerogels

Carbon aerogels or porous carbons synthesized via the sol-gel route, are considered as very interesting materials for high-temperature thermal insulations in non-oxidizing atmospheres or vacuum (Pekala, 1989; Hrubesh & Pekala, 1994). Carbon aerogels are open porous solids consisting of a three-dimensional network of spherical interconnected primary particles. The mean pore and particle size can be specifically adjusted to be in the range from several nanometers only to some microns by varying the synthesis conditions. Porosities up to about 99% can be achieved. These properties make carbon aerogels suitable for thermal insulation applications (Li et.al, 2002; Petricevic et.al, 2001), in particular at high temperatures, but also for electrodes in supercapacitors and gas diffusion layers in fuel cells. Carbon aerogels are often produced using RF (resorcinol and formaldehyde as the main precursors) method. RF polymer precursor was prepared by polycondensation of resorcinol with formaldehyde in an aqueous solution. Sometimes, sodium carbonate, which was used as a base catalyst, was mixed with resorcinol and deionized water, to accelerate dehydrogenation of resorcinol. After stirring the solution for a few minutes, formaldehyde was added slowly into the solution to form a sol.

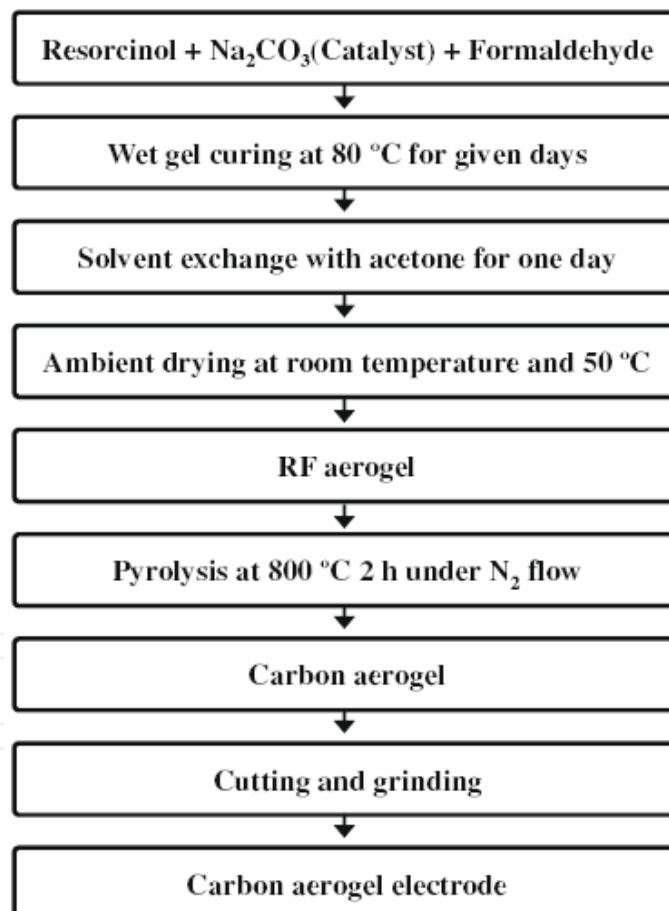


Fig. 4a. Overall preparation route for carbon aerogels Ref (Yoon Jae Lee et.al, 2010)

Yoon Jae Lee et.al (Yoon Jae Lee et.al, 2010) listed typical the processing route for carbon aerogels (see Figure.4a). M.Wiener et.al (Wiener et.al, 2009) investigated the high-temperature insulation properties of carbon-based aerogels derived via pyrolysis of organic aerogel precursors, which were synthesized using resorcinol and formaldehyde as

precursors according to the sol-gel process. The reactants resorcinol and formaldehyde in the starting aqueous solution was adjusted to a mass ratio  $M$  of 25% ( $M$  = mass of resorcinol and formaldehyde to total mass of the solution) to yield a density of the resulting aerogel of about  $230 \text{ kg m}^{-3}$ . After carbon gel formed, the samples were exposed to  $85^\circ\text{C}$  for 24 h for gelling and curing. The pore liquid within the wet gel was replaced by ethanol to reduce the surface tension upon drying. Subsequently, the gels were dried at ambient conditions. Finally the resulting organic aerogels were pyrolyzed in an argon atmosphere at  $1073\text{K}$  and  $2073 \text{ K}$ . Figure.5 shows the microscopic structure of one of the carbon aerogels synthesized.

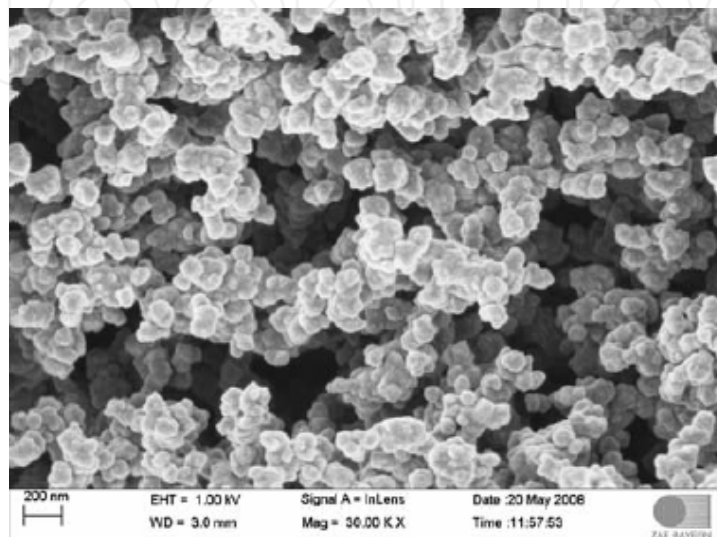


Fig. 5. SEM image of one of the carbon aerogels synthesized ( $T_{\text{pyro}} = 2073 \text{ K}$ ) Ref(Wiener et.al,2009)

The effective thermal conductivities of carbon aerogels according the determined values of thermal diffusivity, specific heat, and sample densities are shown for the two carbon aerogels investigated in Figure. 6. The comparison of the values derived in  $0.1\text{MPa}$  argon atmosphere and under vacuum shows that the difference between the two datasets is almost temperature independent on the order of  $0.02\text{W} \cdot \text{m}^{-1} \cdot \text{K}^{-1}$ . This difference in thermal conductivities represents the contribution of the gas in the pores of the aerogel to the total effective thermal conductivity.

In Figure.7, these data are compared to the experimental data of the total effective thermal conductivities measured in vacuum. The plot reveals that the radiative transport represents even at  $1770\text{K}$  only a small contribution to the total effective thermal conductivity in the carbon aerogel investigated. The thermal transport is rather dominated by the heat transfer via the solid phase. The full line in Figure.7 corresponds to a fit of a superposition of the radiative thermal conductivity and the solid thermal conductivity the upper dashed line in Figure.7 represents the effective thermal conductivity to be expected for a carbon aerogel derived from the same organic precursor as the samples measured here, however, pyrolyzed at a temperature of  $2773 \text{ K}$ . Under  $0.1\text{MPa}$  argon atmosphere, the values are expected to increase by an additional constant term of about  $0.02\text{W m}^{-1} \cdot \text{K}^{-1}$ .

It showed that the thermal conductivity via the backbone of carbon aerogels is strongly increasing with the pyrolysis or the annealing temperature applied (Wiener et.al, 2006); this is due to the increase in ordering of the carbon structure on the molecular scale accompanied by the growth of the carbonaceous microcrystallites. The study revealed that

these structural changes mainly reduce the grain boundaries and thus the scattering of the phonons dominating the heat transport via the solid phase. In contrast, the electronic contribution to the thermal transport was shown to be negligible as expected for highly amorphous systems. Nevertheless, the earlier paper already revealed the high potential of carbon aerogels as high-temperature thermal insulations.

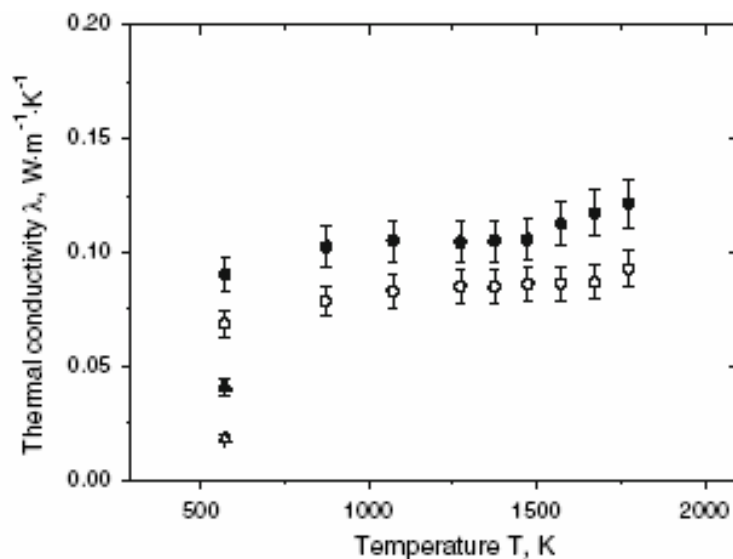


Fig. 6. Thermal conductivity of the investigated carbon aerogel (pyrolysis temperature=2073K) as a function of temperature under 0.1MPa argon atmosphere (filled circle) and vacuum (open circle). Also shown is the thermal conductivity of a carbon aerogel (pyrolysis temperature = 1073K) at 573K in 0.1MPa argon atmosphere (filled triangle) and vacuum (open triangle). Ref(Wiener et.al,2009)

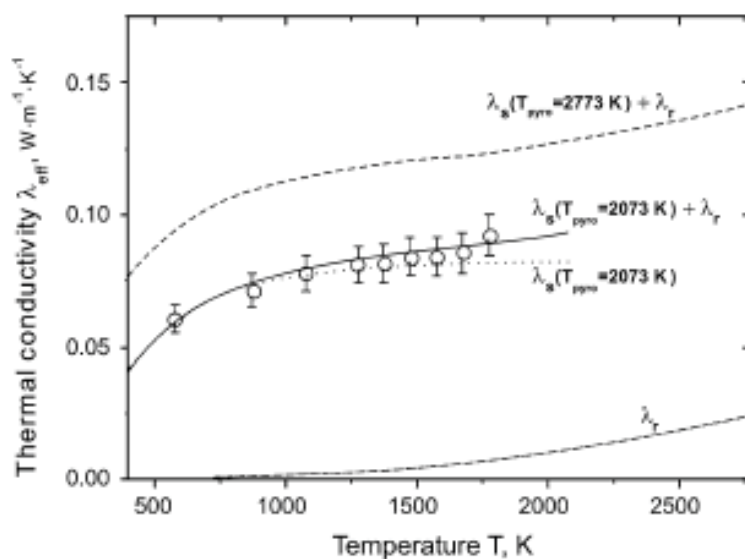


Fig. 7. Thermal conductivities of a carbon aerogel (pyrolysis temperature=2073K) measured as a function of temperature in vacuum (open circle). Radiative  $\lambda_r$  and solid  $\lambda_s$  contributions to the thermal conductivity are indicated; full line represents the superposition of the two terms. Upper dashed line corresponds to the thermal conductivity expected for the same aerogel, however, pyrolyzed at 2773K. Ref(Wiener et.al,2009)

### 2.3 Production of SiO<sub>2</sub>-based aerogels with opacifier addition

Pure Aerogel is poor thermal insulator because it is highly transparent in the special wavelength regions (i.e., from 3 to 8 μm). To improve its thermal insulation capacity, approaches such as doping aerogel with TiO<sub>2</sub>, K<sub>2</sub>Ti<sub>6</sub>O<sub>13</sub> whisker or carbon black could minimize the infrared radiation heat transfer. The opacifier has the ability to suppress radiation transport by eliminating the infrared transparent window of aerogel.

In our previous studies, SiO<sub>2</sub> composite aerogels-doped K<sub>2</sub>Ti<sub>6</sub>O<sub>13</sub> whisker (2–8 wt.% K<sub>2</sub>Ti<sub>6</sub>O<sub>13</sub> in the final aerogel) were prepared according to the acid (HCl)-catalyzed sol-gel procedure. Briefly, tetraethoxysilane (Si(OC<sub>2</sub>H<sub>5</sub>)<sub>4</sub>, Aldrich 98.5%, TEOS), EtOH, HCl and H<sub>2</sub>O with molar ratios of 1:7:4 were used as precursors for the silica. The pH value of above mixture was adjusted to 2 by HCl (0.2 mol/L).

The K<sub>2</sub>Ti<sub>6</sub>O<sub>13</sub> whisker (diameter of 1–2 μm and length of 10–50 μm, 95% purity) was ultrasonically dispersed for 60 min in the TEOS/EtOH/H<sub>2</sub>O mixture. Then the mixture-doped K<sub>2</sub>Ti<sub>6</sub>O<sub>13</sub> whisker was refluxed at 80 °C for 40 min, followed by the addition of 0.25 ml of 0.05 mol NH<sub>3</sub>·H<sub>2</sub>O and mixed for about 10 min until the transparency appear. After 24 h of aging in TEOS/EtOH solution to strengthen the gel network structure, the pore fluids in wet gel were exchanged with ethanol by turns to facilitate following surface modification. Subsequent modification was preceded by immersing wet gel in cyclohexane solution at 30°C for 48 h. Modified wet gel was dried in the oven at 65°C for several days and further heat-treated at increasing temperature up to 500, 700, 800, 900 and 1000°C for 2 h. In this study, the aerogel before the heat-treatment is designated as the “as-dried aerogel.” The mass percentage of K<sub>2</sub>Ti<sub>6</sub>O<sub>13</sub> whisker in total silica-based aerogels was 2% for KT-2, 4% for KT-4, 6% for KT-6, and 8% for KT-8.

As for TiO<sub>2</sub> additive, firstly SiO<sub>2</sub>-TiO<sub>2</sub> gels were prepared with the acid (HCl)-catalyzed sol-gel method by using tetraethoxysilane (TEOS) as precursors, which follows the same trend of chemical reactions of aerogels doped K<sub>2</sub>Ti<sub>6</sub>O<sub>13</sub> whisker. The TiO<sub>2</sub> (TiO<sub>2</sub> KA-100, rutile crystalline phase, mean particle size = 50 nm) nano-powder were firstly ultrasonically dispersed for 60 min in the TEOS/EtOH/HCl/H<sub>2</sub>O mixture. The content of TiO<sub>2</sub> powder is 1, 3, 5 and 10 wt.%, respectively. The detailed processing for preparing aerogels with opacifier addition is listed in Figure.8

## 3. Microstructure

### 3.1 Microstructural and structural feature for SiO<sub>2</sub>-TiO<sub>2</sub> system

Figure.9 shows the microstructure of silica matrix aerogel composite observed by SEM. TiO<sub>2</sub> particles were dispersed within silica aerogel matrices and most TiO<sub>2</sub> particles were adhered to silica network. As the arrows in Figure.9 indicated, there are small irregularly localized white particles with uniform diameters of approximately 50 nm. These nanoparticles are attributed by EDS analysis (not shown here) to titania oxide (TiO<sub>2</sub>) incorporated into silica glass.

TEM micrographs of the obtained aerogels are also presented in Figure.10(a) and (b). It can be observed that silica aerogels exhibit a sponge-like microstructure. The spherical SiO<sub>2</sub> particles with a size of a few tens of nm form a 3-dimensional network containing homogeneous pores (size in the range of 10–15 nm). The HRTEM image, also shown in Figure.10(c), indicates that the spherical TiO<sub>2</sub> particle is embedded into amorphous silica and the interface between silica aerogel and TiO<sub>2</sub> is clean.

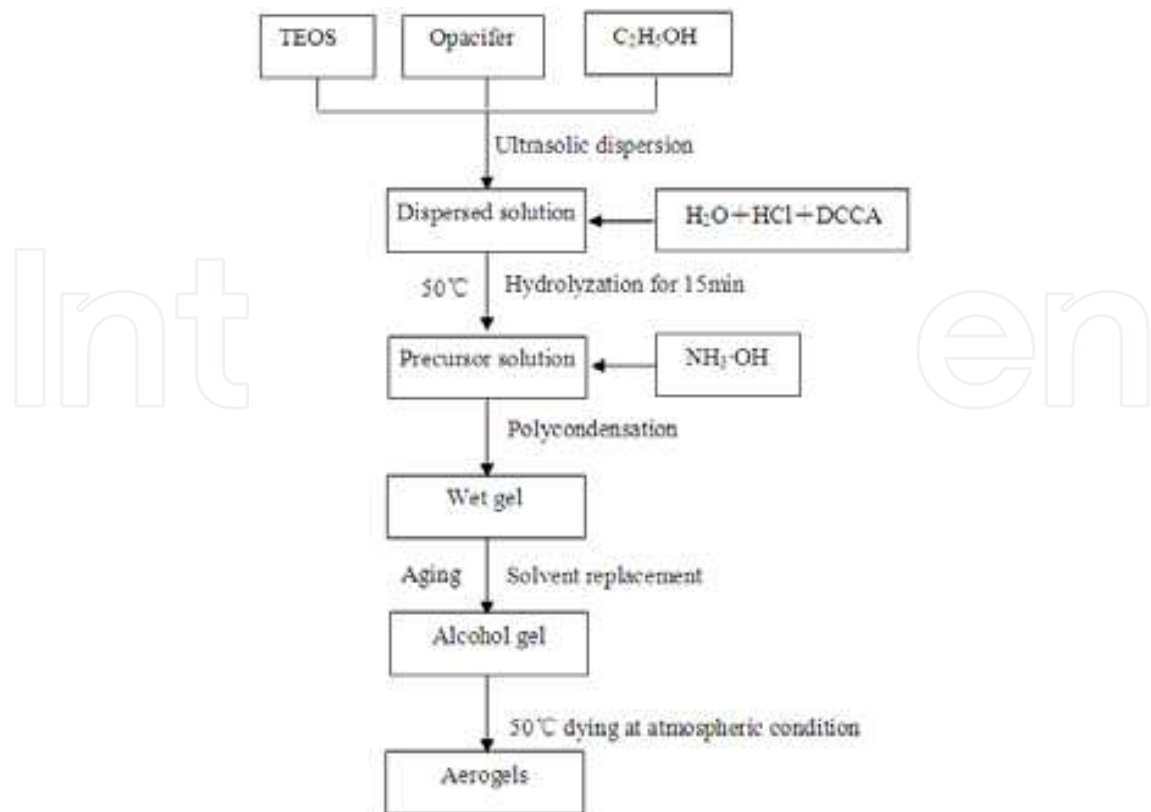


Fig. 8. Processing chart of preparation process of silica based aerogel doped with opacifier additive

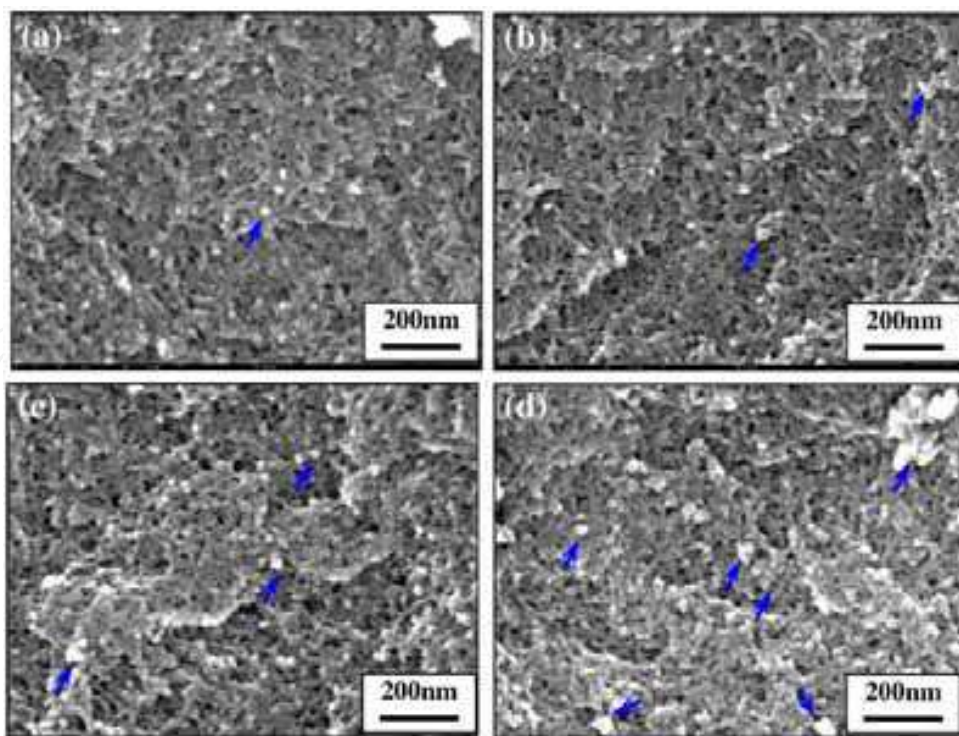


Fig. 9. SiO<sub>2</sub> aerogels doped with different TiO<sub>2</sub> content (a) 1 wt.%; (b) 3 wt.%; (c) 5 wt.%; (d) 8 wt.%.

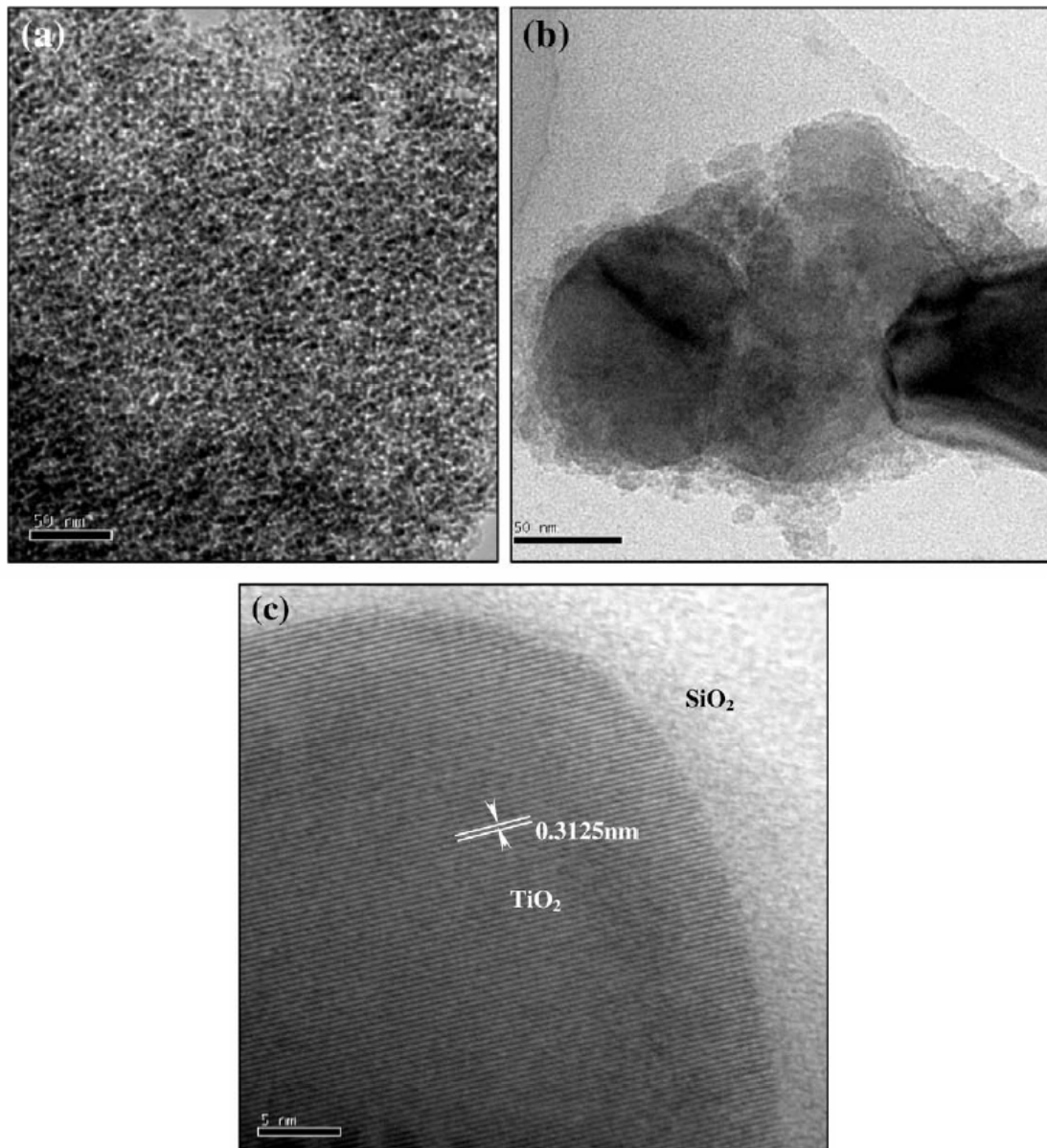


Fig. 10. TEM and HREM of prepared aerogel for ST5 (a) TEM of nano-porous silica aerogel; (b) TiO<sub>2</sub> particle incorporated in silica aerogel; (c) HREM for interface between silica aerogel and TiO<sub>2</sub> particle.

Figure. 11 shows the XRD patterns from ST5 heat-treated ranged from 500 to 1000°C. It could be seen that the presence of amorphous silica appeared as a large band centered at 21°. The crystal peaks were found during the whole temperature ranges due to the addition of TiO<sub>2</sub> and all of the TiO<sub>2</sub> peaks are rutile phase. FTIR spectra of the prepared silica aerogel and ST5 heat-treated at different temperature are indicated in Figure.12 and 13, respectively. The peaks at 3400 and 1644 cm<sup>-1</sup> correspond to the O-H absorption band, which is caused by physically adsorbed water. The peaks near 460, 800, and 1091 cm<sup>-1</sup> are due to Si-O-Si bending modes, symmetric Si-O-Si stretching vibration and asymmetric Si-O-Si stretching vibration, respectively. Additionally, the bands at 2920 and 1400 cm<sup>-1</sup> were assigned to C-H vibrations. The latter C-H could be attributed to organic residues, which remained in prepared aerogels even after calcinations.

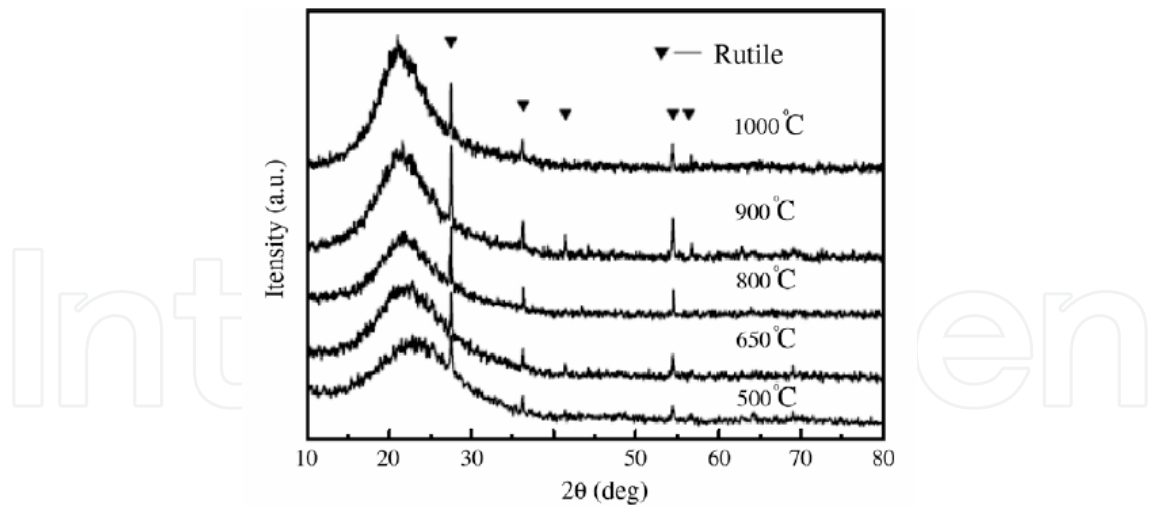


Fig. 11. XRD patterns of ST5 according to various heat-treatment temperature.

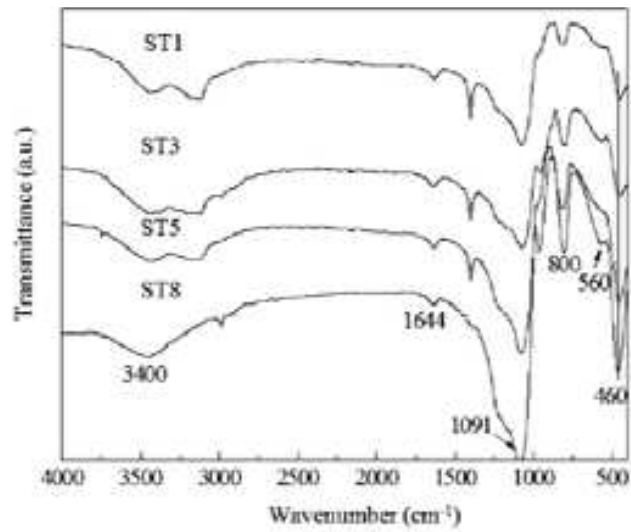


Fig. 12. FTIR spectra of composite silica aerogels according to various  $\text{TiO}_2$  additives.

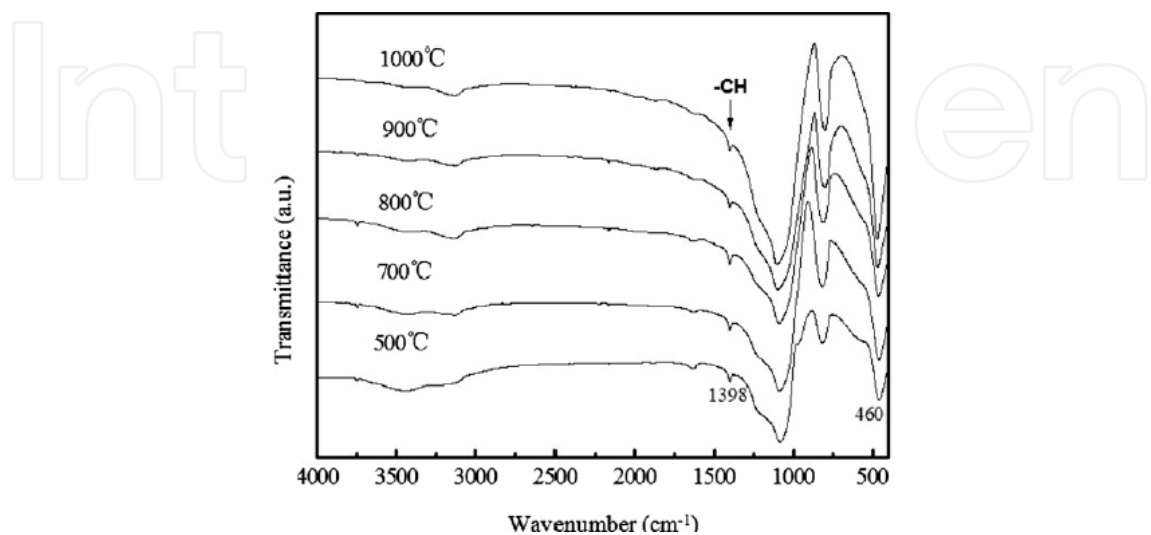


Fig. 13. FTIR spectra of ST5 heat treated at different temperature.

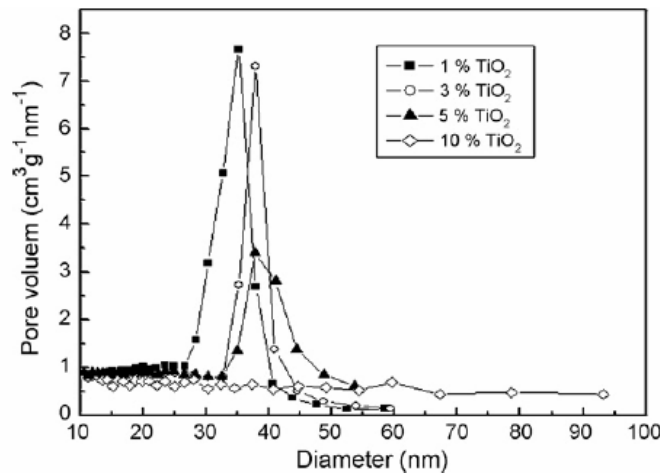


Fig. 14. Pore radius distribution of SiO<sub>2</sub> aerogels with different TiO<sub>2</sub> content

The peak of pore size distribution increased with the more TiO<sub>2</sub> additive (see Figure.14). It is observed that for all the samples the pore size distribution curves are in the range 10–60 nm with a relative narrow pore distribution centred around 30–45 nm. The pore diameter of ST1 was the minimum. Then as the TiO<sub>2</sub> content increased, the pore diameter increased slightly. It is known that aerogels are mainly comprised of mesopores below 50 nm. Considering the maxim pore size had exceeded 2 $\mu$ m by nitrogen adsorption and desorption method (Table.2), silica composite aerogel could have macropores larger than 2 $\mu$ m. The fact is supported by smaller pore volume and specific surface area for ST10.

Sample	Pore volume (cm <sup>3</sup> /g)	$d_{max}$ (nm)	Specific surface area(m <sup>2</sup> /g)	$d_{average}$ (nm)
1%TiO <sub>2</sub>	1.219	318.53	1210	30.28
3%TiO <sub>2</sub>	0.985	2999.3	1026	38.42
5%TiO <sub>2</sub>	1.040	3398.8	1089	38.20
10%TiO <sub>2</sub>	0.898	2235.3	785	45.73

Table 2. Properties of SiO<sub>2</sub>-TiO<sub>2</sub> aerogels obtained via ambient pressure drying

Figure.15 shows the nitrogen adsorption–desorption isotherm of silica doped TiO<sub>2</sub> aerogels. The ST1, ST3 and ST5 samples exhibit typical type-IV adsorption isotherms, which are considered to indicate the presence of mesopores. There are shifts in the loops, but the basic shape seems to be constant. All the adsorption of N<sub>2</sub> increases first, and then decreases with a maximum at ST1 due to more capillary condensation in the mesopores, which gives the larger surface area. Compared with the ST1, ST3 and ST5, the ST10 aerogels exhibit type-II adsorption isotherms and the ST10 sample has low adsorption and almost no hysteresis. Because higher TiO<sub>2</sub> content may lead to the TiO<sub>2</sub> agglomeration during sol–gel process, and these agglomeration will close some mesopores and cause the breakage between the SiO<sub>2</sub> and TiO<sub>2</sub> interface in local area, which is reflected in the lower surface area and lower pore volume. Generally the SiO<sub>2</sub> aerogel possesses the potential to form a highly porous structure, giving large surface area and pore volume. While mixing TiO<sub>2</sub> into SiO<sub>2</sub> aerogel, the textural properties of the composite aerogels may change due to the interaction between them. The specific surface area of the aerogels slightly decreased, from 1210m<sup>2</sup>/g for the ST1 to about 785m<sup>2</sup>/g for ST10. The pore volume of the composite aerogels changes slowly, decreasing from 1.219 cm<sup>3</sup>/g for ST1 to 0.898 cm<sup>3</sup>/g for ST10. The decreasing of the pore volume is due

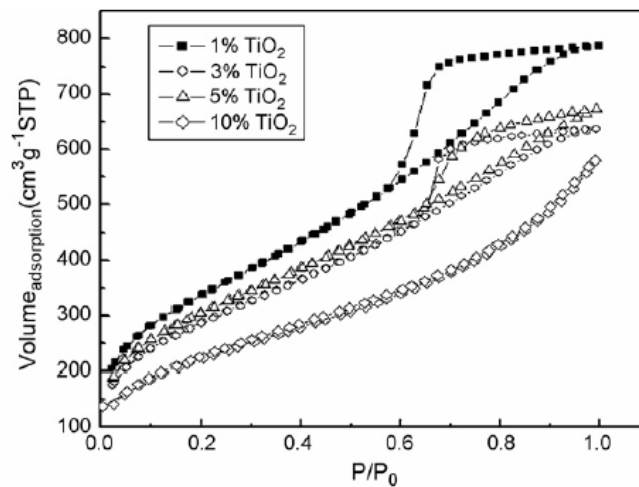


Fig. 15. BET of SiO<sub>2</sub> aerogels with different TiO<sub>2</sub> content

to the enhancement of the pore size in both the micropore and mesopore ranges due to the incorporation of TiO<sub>2</sub> into the framework of SiO<sub>2</sub>.

### 3.2 Microstructural and structural feature of SiO<sub>2</sub>-K<sub>2</sub>Ti<sub>6</sub>O<sub>13</sub> whisker composite aerogels

Figure.16 shows the microstructure of silica matrix aerogels composite observed by SEM. K<sub>2</sub>Ti<sub>6</sub>O<sub>13</sub> whisker were dispersed within silica aerogel matrices and most K<sub>2</sub>Ti<sub>6</sub>O<sub>13</sub> whisker were adhered to silica aerogels. When silica aerogel parts were magnified, 10–20nm sized pores and 10–30nm sized spherical solid clusters were known to be existed. TEM micrographs of the obtained aerogels are also presented in Figure.17. It can be observed that silica aerogels exhibit a sponge-like microstructure. The spherical SiO<sub>2</sub> particles with a size of a few tens of nanometers form a three-dimensional network containing homogeneous pores (size in the range of 10–15 nm).

Figure.18 shows the XRD patterns for KT-6 heat-treated at different temperatures. It could be seen that the aerogels were amorphous below 800°C and only some negligible K<sub>2</sub>Ti<sub>6</sub>O<sub>13</sub> crystal peaks were found around 25.4°. However, XRD patterns show halo in the range of 20–22° corresponded to the characteristic peaks of silica crystalline and K<sub>2</sub>Ti<sub>6</sub>O<sub>13</sub> up to 900°C. It can be concluded that the phase transformation for silica aerogel might occur from amorphous phase to crystalline state above 800°C.

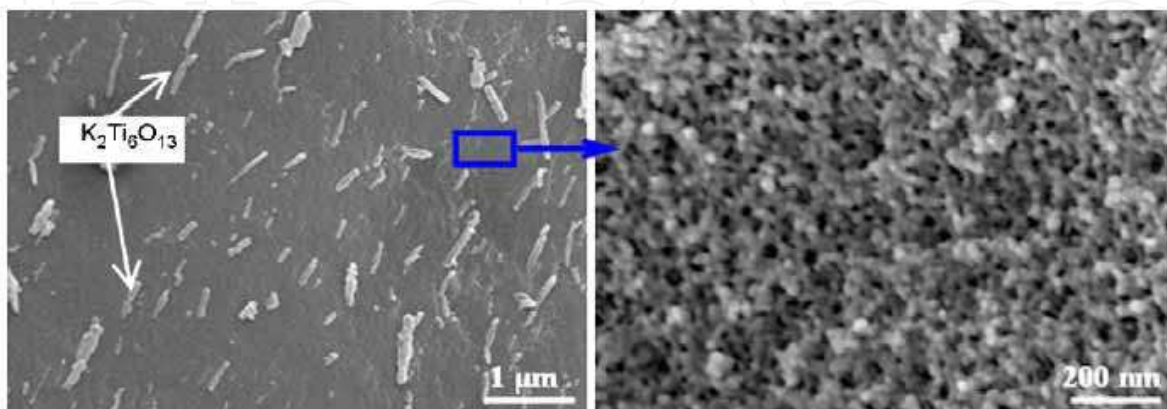


Fig. 16. SEM photographs of silica aerogel composite (left) and magnified silica aerogel part (right).

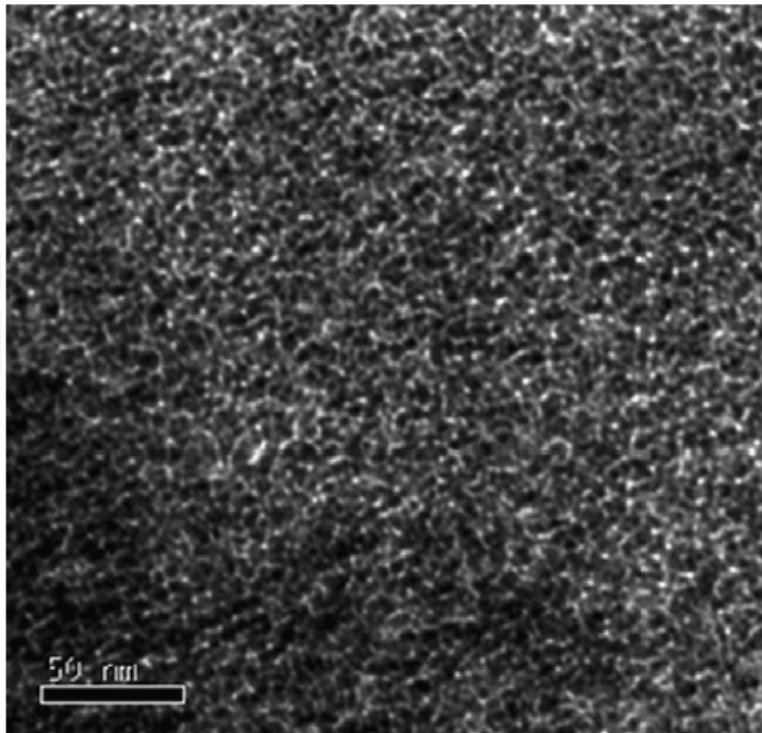


Fig. 17. TEM image of silica aerogel parts in SiO<sub>2</sub>- K<sub>2</sub>Ti<sub>6</sub>O<sub>13</sub> system

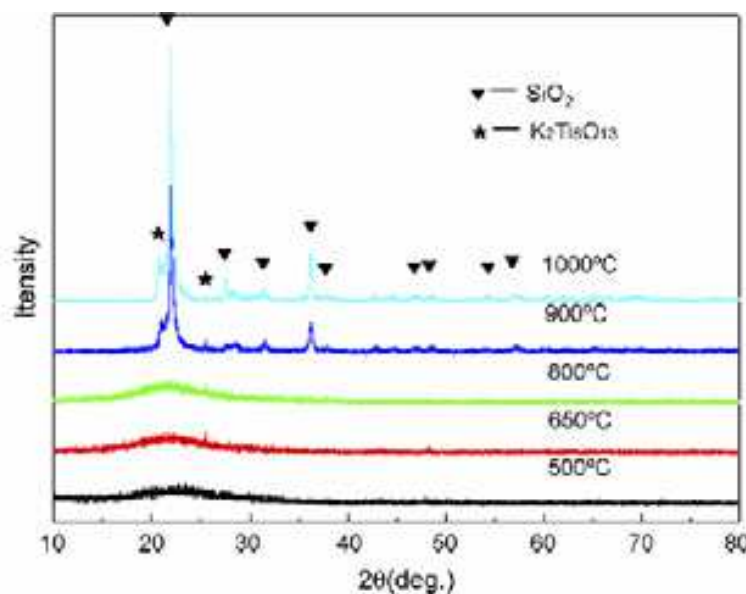


Fig. 18. XRD patterns of KT-6 according to various heat-treatment temperatures

FTIR spectra of the prepared silica aerogel are indicated in Figure.19. The peaks at 3438 and 1630cm<sup>-1</sup> correspond to the O-H absorption band, which is caused by physically adsorbed water. The absorption peaks near 1091 and 460cm<sup>-1</sup> are due to Si-O-Si vibrations, which will appear in any silica products. It is obvious that apart from Si-O-Si and O-H absorption peaks, the absorption peaks at 1395 and 825cm<sup>-1</sup> correspond to Si-C bonding. The spectrum shows almost the same patterns, irrespective of the additive of K<sub>2</sub>Ti<sub>6</sub>O<sub>13</sub> whisker. Even though the aerogels are chemically identical, there are differences in their physical properties, such as their transmittance, density and thermal stability.

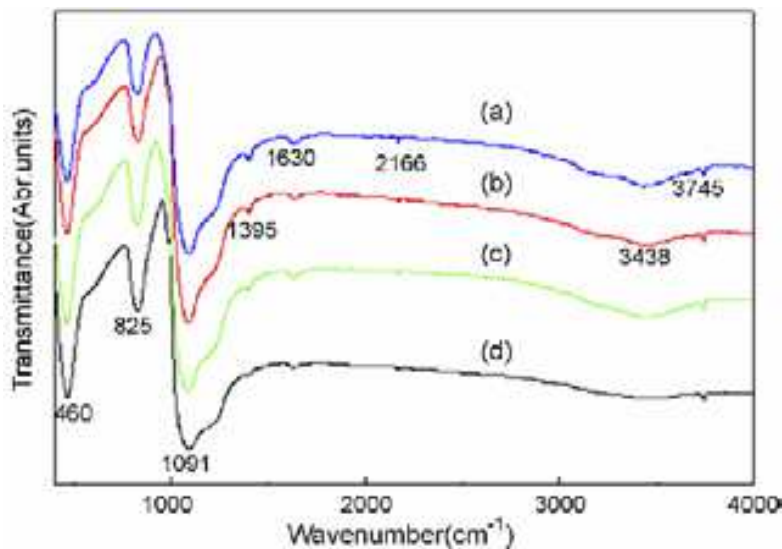


Fig. 19. FT-IR spectra of composite silica aerogels according to various  $K_2Ti_6O_{13}$  whisker additive (a) KT2; (b) KT4; (c) KT6; and (d) KT8.

#### 4. Thermal properties of $SiO_2$ -based aerogels

As the investigations described here are mainly performed in order to develop new thermal insulation materials for application at higher temperatures (mainly between 25 and 800°C), the aerogels were characterized with respect to their infrared transmittance in the wavelength range from 2.5 to 12  $\mu m$ . For larger wavelengths (>10  $\mu m$ ) the transmittance of the  $SiO_2$  skeleton is in the range of 65% (Figure. 20) and thus dominates the transmittance spectrum. As is evident in Figure.20, the infrared spectra of all of the samples demonstrate that with decreasing  $K_2Ti_6O_{13}$  additive there is a decrease in transmittance. This is caused by the increase in the scattering intensity according to the Rayleigh relation. For all different contents of  $K_2Ti_6O_{13}$  additive, the transmittances of the aerogels increased slowly with increasing wavelength ranging from 2 to 7  $\mu m$ . The transmittance of the prepared aerogel for KT-2 was about 50% at a wavelength in the range of 4–7  $\mu m$ , while it was only 15% for the aerogel for KT-8. This difference seems to emanate from variations in the microstructure, such as the morphological change of the pores in the aerogel network structure. For a given density of silica, the microstructure, especially the secondary particle (cluster) content and size, play an important role in determining the transmittance of the silica aerogel (Zhang et al., 2009). On the other hand, most infrared wavelengths were blocked by the aerogels, regardless of the additive of  $K_2Ti_6O_{13}$  whisker, so that over 55–85% of the waves were interrupted at a wavelength of around 5–7  $\mu m$ .

Previous studies (Wang et al., 1995) showed that the additive of  $TiO_2$  led to a strong increase of the specific extinction and thus decrease of the radiative thermal conductivity at high temperature.  $K_2Ti_6O_{13}$  whisker has a high-reflection index and negative temperature thermal conductivity (i.e., exhibiting a thermal conductivity of 0.089 and 0.017 W/mK at 30 and 800°C, respectively) [Wang et al., 2005]. Thus more absorbing energy could be blocked, thereby resulting in a decrease in the transmittance with the increasing of additive of  $K_2Ti_6O_{13}$  whisker.

Figure.21 shows the transmittance variation for the composite aerogels at different temperatures. It can be seen that the transmittance also changed according to the different

additives of K<sub>2</sub>Ti<sub>6</sub>O<sub>13</sub> whisker. The composite aerogels heated to temperatures at 300°C showed a transmittance of about 35% for the near 3 μm wavelength, whereas those heat-treated at more than 400°C blocked over 95% of the near the same waves. As is evident in Figure.21, the transmittance gradually decreased as the heat-treatment temperature was increased up to 600°C. According to the FT-IR and TG/DTA results, the hydrophobic surface groups disappeared and the aerogel became hydrophilic at temperatures above 320°C. Thus, the adsorption and desorption of the hydrophobic functional groups seems to be responsible for the optical behavior of the aerogels.

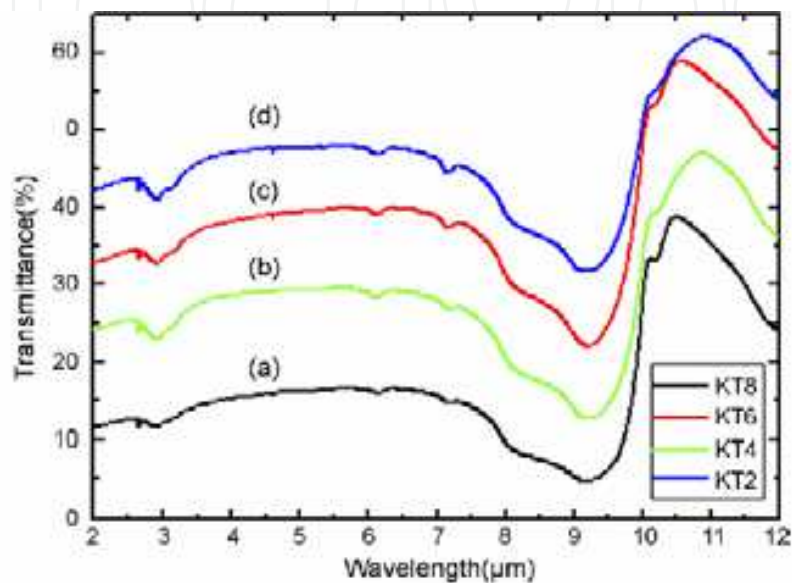


Fig. 20. Transmittance of the composite silica aerogels in the infrared light region. The aerogels were prepared with different K<sub>2</sub>Ti<sub>6</sub>O<sub>13</sub> whisker additive (a) KT8; (b) KT6; (c) KT4; and (d) KT2.

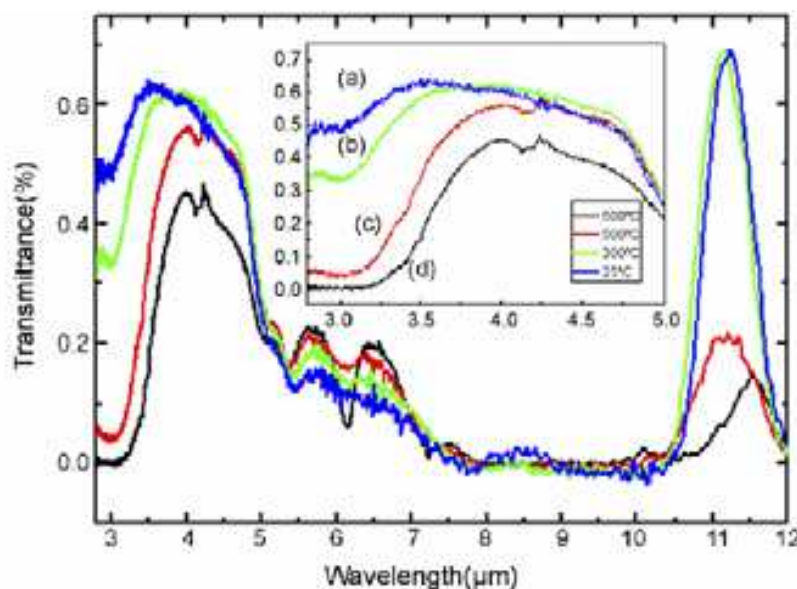


Fig. 21. Transmittance of the composite silica aerogels with KT6 additive heated at different temperatures (a) 100°C; (b) 350°C; (c) 500°C; and (d) 600°C.

TiO<sub>2</sub> is another important opacifier to increase the thermal property for aerogels. As is evident in Figure.22, the infrared spectra of all of the samples demonstrate that with TiO<sub>2</sub> additive there is a decrease in transmittance. The optical properties measured here show that the transmittance of the pure SiO<sub>2</sub> aerogel is relative high (about 60%) on the whole range of wavelengths. The transmittance of the prepared aerogel for ST1 was near to 50% at a wavelength in the range of 3–8μm, while it was below 40% for the aerogel for ST5 and ST8. Figure.23 shows the transmittance variation for pure silica aerogel and ST5 at 500°C. It can be seen that the pure aerogel even remains a high optical transmittance (exceeding 60%). Meanwhile the transmittance for ST5 was comparably decreased, especially ranging from 5 to 8μm (i.e., far below 30%). It is clear that additive of TiO<sub>2</sub> can greatly decrease the transmittance in room temperature as well as in high temperature. Previous reported literature also showed that the effective specific extinction increased with the amount of TiO<sub>2</sub> (Zhang et.al, 2010), and thus the radiative thermal conductivity or the infrared transmittance is certainly reduced, which can also be described by Rayleigh scattering theory. Usually the resulted silica aerogels are transparent, and this is because the aerogel microstructure has a small scale compared to the wavelength of light. Their transparency plays an important role in high energy physics with charged particles, while their optical transparency should be reduced for thermal insulation application.

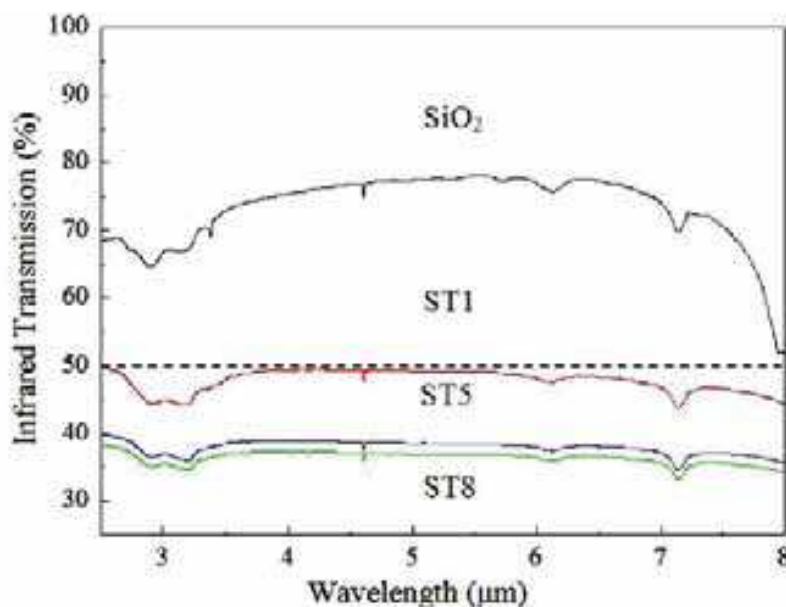


Fig. 22. Transmittance of silica aerogels prepared with different TiO<sub>2</sub> opacifier

From above experimental analysis and discussion, it can be seen that transmittance of the prepared aerogels strongly depend on the opacifier content as well as the spectral wavelength. By contrast, the pure aerogels exhibits radiative properties which are remarkably stable, remaining high transmittance in the range of investigated wavelengths. Such a feature is characteristic of so-called transparent materials. Given its relatively higher transmittance, aerogel doped with TiO<sub>2</sub> or K<sub>2</sub>Ti<sub>6</sub>O<sub>13</sub> opacifier is a semi-transparent material with a low transmittance.

The value of thermal conductivity of SiO<sub>2</sub>-based aerogels is listed in Table.3. For K<sub>2</sub>Ti<sub>6</sub>O<sub>13</sub> whisker addition, the total thermal conductivity decreased gradually with the increasing of K<sub>2</sub>Ti<sub>6</sub>O<sub>13</sub> whisker, which is due to the very low thermal conductivity of K<sub>2</sub>Ti<sub>6</sub>O<sub>13</sub> whisker.

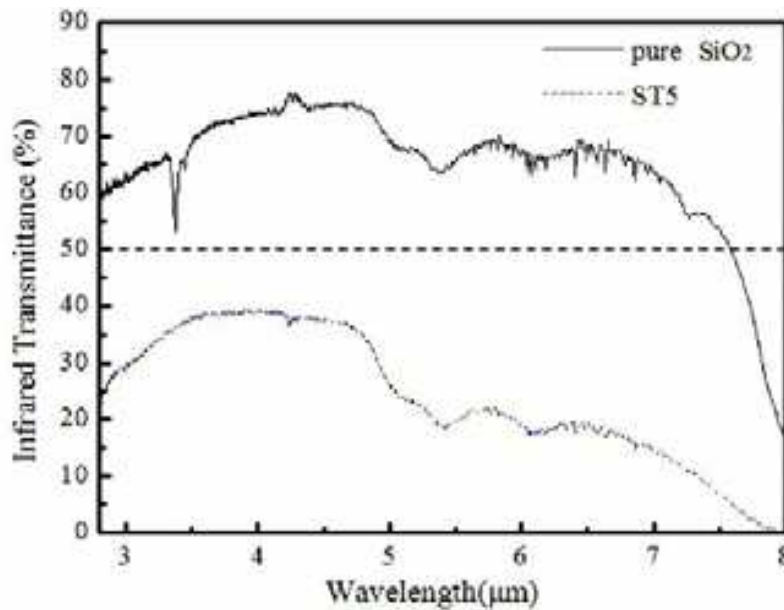


Fig. 23. Transmittance of silica aerogels and ST5 at 500°C

While for TiO<sub>2</sub> addition, the thermal conductivity increased with the more content of TiO<sub>2</sub> addition. Because TiO<sub>2</sub> could increase the total thermal conductivity at room temperature, however, this is might be reverse at higher temperature.

Sample	Bulk density (gcm <sup>-3</sup> )	Pore size (nm)	Thermal conductivity (Wm <sup>-1</sup> K <sup>-1</sup> )
SiO <sub>2</sub> aerogels	1250	26.3	0.060
KT2	843	27.6	0.057
KT4	741	27.9	0.055
KT6	688	27.7	0.054
KT8	694	29.5	0.051
ST1	1210	30.28	0.061
ST3	1026	38.42	0.063
ST5	1089	38.20	0.065
ST10	785	45.73	0.072

Table 3. Thermal conductivity of SiO<sub>2</sub>-based aerogels

## 5. Summary and future perspectives

Aerogels have a wide variety of exceptional properties, hence a striking number of applications have developed for them. Many of the commercial applications of aerogels such as catalysts, thermal insulation, windows, and particle detectors are under development and new applications have been developed, but little in the way of actual use has resulted (Soleimani Dorcheh & Abbasi, 2008;). However, monolithic silica aerogel has been used extensively in high energy physics in Cherenkov radiation detectors. Other application of silica aerogels are: shock wave studies at high pressures, inertial confinement fusion (ICF), radioluminescent devices and micrometeorites (Barbieri et.al, 2001; Beck et.al, 1989; Bhagat, et.al, 2006; Bhagat, et.al, 2007; Bisson, et.al, 2004).

Property	Features	Application
Thermal conductivity	<ul style="list-style-type: none"> <li>• Best insulating solid</li> <li>• Transparent</li> <li>• High temperature</li> <li>• Lightweight</li> </ul>	<ul style="list-style-type: none"> <li>• Architectural and appliance insulation, transport vehicles, pipes</li> <li>• Space vehicles and probes, casting molds</li> </ul>
Density /porosity	<ul style="list-style-type: none"> <li>• Lightest synthetic solid</li> <li>• Homogeneous</li> <li>• High specific surface area</li> </ul>	<ul style="list-style-type: none"> <li>• Catalysts, sorbers, sensors fuel storage, ion exchange</li> <li>• Targets for ICF, X-ray lasers</li> </ul>
Optical	<ul style="list-style-type: none"> <li>• Low refractive index solid</li> <li>• Transparent</li> <li>• Multiple compositions</li> </ul>	<ul style="list-style-type: none"> <li>• Cherenkov detectors, lightweight optics, lightguides, special effect optics</li> </ul>
Acoustic	<ul style="list-style-type: none"> <li>• Lowest sound speed</li> </ul>	<ul style="list-style-type: none"> <li>• Impedance matchers for transducers, range finders, speaker</li> </ul>
Electrical	<ul style="list-style-type: none"> <li>• Lowest dielectric constant</li> <li>• High dielectric strength</li> <li>• High surface area</li> </ul>	<ul style="list-style-type: none"> <li>• Dielectrics for ICs, spacers for vacuum electrodes, vacuum display spacers, capacitors</li> </ul>

Table 4. Property, features and application of aerogels

It is interesting to compare the various exceptional properties and features of aerogels with their real or prospective applications. This gives an idea of the tremendous variety of aerogel applications and hints at the impact that these materials will have as we view their future uses. Table 3 lists some possible applications, both general and specific, which result from particular properties of the aerogels.

Although there are many challenging problems to be solved before the application of aerogels, it has verified that aerogels as a class of materials, have already demonstrated an incredible versatility of applications; probably having no comparable competitor in recent years. It can be said that the full impact of these materials for public use is yet to come. It is doubtful that it will happen until the cost of producing these materials is reduced and the price becomes competitive with other polymer materials. While this may still be a few years away, the authors believe that the common use and availability of aerogels is inevitable.

## 6. Conclusion

This chapter provides a comprehensive introduction of the synthesis, structure, thermal properties and characterization of silica aerogels. Aerogels show great promise for use in variety of technological areas where special structure and physical properties are required. Substantial progress has been made in the development, processing and characterization of areogel materials over the recent years. Special attention has been paid to the use of inexpensive precursors and the drying technology to make the production commercial.

Silica aerogel synthesis with various materials and process conditions and also the properties and method determination are reviewed and supplied in this chapter.

## 7. References

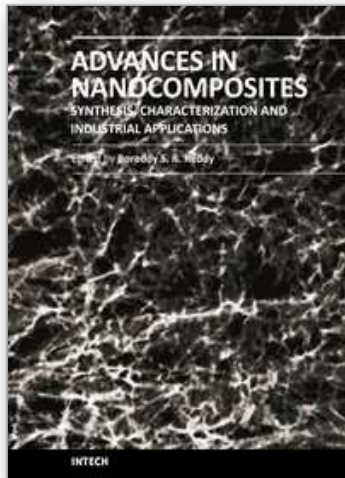
- Muller, C.A.; Maciejewski, M; Mallat, T; Baiker, A. (1999). *J. Catal.* Vol. 184, 280-284
- Hrubesh, L.W.; Coronado, P. R.; Satcher, J. H. (2001). *J. Non-Cryst. Solids.* Vol. 285, 328-332
- Kim, G.S.; Hyun, S.H. (2003). *J. Non-Cryst. Solids.* Vol. 320, 125-129
- Lu, X.; Wang, P. ; Buttner, D.; Heincmann, U.; Nilsson, O.; Kuhn, J. (1991). *High Temp.-High Press.* Vol. 23, 431-435
- Fricke, J.; Lu,X.; Wang, P.(1992). *J. Heat. Mass.Transfer.* Vol. 35, 2305-2309
- Kuhn, J.; Gleissner, T.; Arduini-schuster, M.C.; Korder, S.; Fricke,J. (1995). *J.Non-Cryst. Solids.* Vol. 186, 291-293
- Chadwick, A.V.; Mountjoy, G.; Nield, V.M. (2001). *Chem. Mater.* Vol.13, 1219-1223
- Yoda, S.; Tasaka, Y.; Uchida, K; Kawai, A.; Ohshima,S.; Ikazaki,F.(1998). *J.Non-Cryst. Solids.* Vol. 225, 105-110
- Klementiev, K.V.(2001). *Appl. Phys.* Vol. 34, 209-214
- Reim,M.; Reichenauer, G.; Korner,W.; Manara,J.; Arduini-Schuster,M.; Korder,S.; Beck,A.; Fricke,J. (2004) *J. Non-Cryst. Solids.* Vol. 350,358-363
- Kwon, Y.G.; Choi, S. Y. (2000). *J. Mater. Sci.* Vol. 35, 6075-6079
- Fricke, J.; Tillotson, T. (1997). *Thin Solid Films.* Vol.297, 212-216.
- Zhang, H.X.; He, X.D.; He, F. (2009). *Journal of Alloys and Compounds,* Vol. 472, 194-197
- Wang, J.; Kuhn, J.; Lu, X. (1995) *J. Non - Cryst. Solids.* Vol. 186, 296-300
- Wagh, P.B.; Begag,R.; Pajonk,G.M.(1999).*Materials Chemistry and Physics.* Vol . 57, 214-218
- Sarawade, P.B.; Kim, J.K.; Hilonga,A.; Kim, H.T.(2010). *Solid state Science,* Vol. 12 ,911-918
- Pekala, R.W.(1989).*J.Mater.Sci.*Vol.24,3221-3224
- Hrubesh, L.W.; Pekala R.W.(1994).*J.Mater.Res.* Vol.9, 731-735
- Li, W.C.; Reichenauer,M.(2002).*Carbon,*Vol.40, 2955-2959
- Petricovic,R.;Gloria,M.;Fricke,J.(2001).Vol.39, 857-860
- Lee,Y.J.; Jung, J.C.; Yi,J.; Baeck,S.H.; Yoon,J.R.; Song I.K.(2010).*Current Applied Physics,*Vol.10,682-686
- Wiener,M.; Reichenauer,G.; Braxmeier,S.; Hemberger, F.; Ebert, H.P.(2009). *Int.J.Thermophys.* Vol.30,1372-1385
- Wiener,M.; Reichenauer,G.; Hemberger, F.; Ebert, H.P.(2006). *Int.J.Thermophys.*Vol.27,1826-1831
- Wang, Y. A. ; Yang, J. J.; Zhang, J. W.; Liu, H.J.; Zhang, Z. J. (2005). *Chem Lett .*Vol. 34 , 1168-1173
- Zhang, H.X.; Qiao, Y.J.; Zhang, X.H.; Fang,S.Q.(2010). *J.Non-Cryst.Solids,*Vol.356, 879-883
- Soleimani Dorcheh, A.; Abbasi, M. H. (2008).*Journal of Materials Processing Technology.* Vol. 199, 20-26
- Barbieri, O.; Ehrburger-Dolle, F.; Rieker, T.P.; Pajonk, G.M.; Pinto,N.; Rao, A.V.(2001). *J. Non-Cryst. Solids.* Vol. 285, 109-113.
- Beck, Caps, R., Fricke, J. (1989). *J. Phys. D.*Vol. 22, 730-735.
- Bhagat, S.D., Kim, Y.-H., Ahn, Y.-S., Yeo, J.-G.(2006). *Microporous Mesoporous Mater.* Vol. 96, 237-244.

Bhagat, S.D., Kim, Y.-H., Ahn, Y.-S., Yeo, J.-G.(2007). Applied Surface Science. Vol. 253, 3231–3236.

Bisson, A., Rodier, E., Rigacci, A., Lecomte, D., Achard, P.(2004). J.Non-Cryst. Solids.Vol.350, 230–237.

IntechOpen

IntechOpen



## **Advances in Nanocomposites - Synthesis, Characterization and Industrial Applications**

Edited by Dr. Boreddy Reddy

ISBN 978-953-307-165-7

Hard cover, 966 pages

**Publisher** InTech

**Published online** 19, April, 2011

**Published in print edition** April, 2011

Advances in Nanocomposites - Synthesis, Characterization and Industrial Applications was conceived as a comprehensive reference volume on various aspects of functional nanocomposites for engineering technologies. The term functional nanocomposites signifies a wide area of polymer/material science and engineering, involving the design, synthesis and study of nanocomposites of increasing structural sophistication and complexity useful for a wide range of chemical, physicochemical and biological/biomedical processes. "Emerging technologies" are also broadly understood to include new technological developments, beginning at the forefront of conventional industrial practices and extending into anticipated and speculative industries of the future. The scope of the present book on nanocomposites and applications extends far beyond emerging technologies. This book presents 40 chapters organized in four parts systematically providing a wealth of new ideas in design, synthesis and study of sophisticated nanocomposite structures.

### **How to reference**

In order to correctly reference this scholarly work, feel free to copy and paste the following:

Hexin Zhang, Changqing Hong and Yingjie Qiao (2011). Synthesis, Structural and Thermal Properties of Nano-porous SiO<sub>2</sub>-based Aerogels, *Advances in Nanocomposites - Synthesis, Characterization and Industrial Applications*, Dr. Boreddy Reddy (Ed.), ISBN: 978-953-307-165-7, InTech, Available from: <http://www.intechopen.com/books/advances-in-nanocomposites-synthesis-characterization-and-industrial-applications/synthesis-structural-and-thermal-properties-of-nano-porous-sio2-based-aerogels>

**INTECH**  
open science | open minds

### **InTech Europe**

University Campus STeP Ri  
Slavka Krautzeka 83/A  
51000 Rijeka, Croatia  
Phone: +385 (51) 770 447  
Fax: +385 (51) 686 166  
[www.intechopen.com](http://www.intechopen.com)

### **InTech China**

Unit 405, Office Block, Hotel Equatorial Shanghai  
No.65, Yan An Road (West), Shanghai, 200040, China  
中国上海市延安西路65号上海国际贵都大饭店办公楼405单元  
Phone: +86-21-62489820  
Fax: +86-21-62489821

© 2011 The Author(s). Licensee IntechOpen. This chapter is distributed under the terms of the [Creative Commons Attribution-NonCommercial-ShareAlike-3.0 License](#), which permits use, distribution and reproduction for non-commercial purposes, provided the original is properly cited and derivative works building on this content are distributed under the same license.

IntechOpen

IntechOpen